Supplementary Information

Emerging effects of oxygen accumulation on orbital torque

Junyeon Kim, Jun Uzuhashi, Dongwook Go, Daegeun Jo, Tadakatsu Ohkubo, Seiji Mitani, Hyun-Woo Lee, YoshiChika Otani

S1. Consideration on the asymmetric Lorentzian for the ST-FMR spectra

As depicted by Eq. (1) in the main text, we evaluate the OT by the ST-FMR technique with the composition ratio analysis. ST-FMR spectra are decomposed to the symmetric (V_S) and anti-symmetric (V_A) Lorentzian as described by following equations,

$$V_S = -\frac{1}{4}\frac{dR}{d\varphi}\frac{\gamma I_{rf}\cos\varphi}{\Delta 2\pi(df/dH)|_{H_{ext}=H_0}}\frac{\hbar}{2e}\frac{\theta J_C}{4\pi M_S t_{FM}}F_S(H_{ext}) \quad \text{(S1a)}$$

$$V_A = -\frac{1}{4}\frac{dR}{d\varphi}\frac{\gamma I_{rf}\cos\varphi}{\Delta 2\pi(df/dH)|_{H_{ext}=H_0}}\left[\frac{\hbar}{2e}\frac{\theta_{FLT} J_C}{4\pi M_S t_{FM}} + \frac{J_C d_{Cu}}{2}\right]F_A(H_{ext}) \quad \text{(S1b)}$$

where R is the resistance, φ the azimuthal angle, Δ the linewidth, γ the gyromagnetic ratio, I_{rf} the injected charge current, e the elementary charge, θ (θ_{FLT}) the torque efficiency of the anti-damping (field-like) torque, H_{ext} the applied external field, H_0 the resonance field, J_C the current density of the injected charge current, $4\pi M_s$ the saturation magnetization, and t_{FM} (d_{Cu}) the thickness of FM (Cu) layer, respectively. Equation S1a (S1b) presents that the symmetric (anti-symmetric) Lorentzian is determined by the anti-damping (field-like and Oersted field) torque. Here we should carefully consider V_A since θ evaluation by Eq. (1) is affected by nonzero θ_{FLT}. In our previous study, we conclude that θ_{FLT} in the CoFe/Cu/Al_2O_3 structure is negligible through an alternative approach[1]. In this study, we concern θ_{FLT} dependence on the exposure time which could give a failure of the analysis based on Eq. (1). We thus consider tendency of V_S and V_A as a function of the exposure time.

Firstly, we consider resistance dependence on the azimuthal angle which is directly associated with dR/dφ in Eq. (S1). In other words, we observe total magnetoresistance (MR) defined by addition of the anomalous MR (AMR) and the Edelstein MR (EdMR)[2]. As shown in Fig. S1(a), the total MR ratio for the Series 10.5 is almost independent of the exposure time. Except Δ and unknown parameters (θ, θ_{FLT}), all the parameters in right side of Eq. S1 shows negligible variation dependent on the exposure time. Next, we consider $V_S\Delta$ and $V_A\Delta$ which directly reveals θ and θ_{FLT} dependence on the exposure time. $V_S\Delta$ is greatly varied by the exposure time (Fig. S1(b)) whereas variation of $V_A\Delta$ is negligible (Fig. S1(c)). The negligible variation of $V_A\Delta$ is commonly shown for other Series. Thus we conclude that the θ dependence on the exposure time presented in main text is dominantly originated from the variation of the anti-damping torque rather than that of the field-like torque.

S2. Spin/OAM pumping and inverse orbital Edelstein effect

A recent report argues generation of the charge current by the spin/OAM pumping via inverse orbital Edelstein effect (IOEE)[3]. The consideration of the spin/OAM pumping and the IOEE is necessary since the charge current by the IOEE could bring an additional voltage for ST-FMR spectra[4]. Figure S2 presents generated voltage by the spin/OAM pumping for selected samples among the Series 10.5. Here there is no sample which presents a considerable voltage peak, meaning a negligible impact by the IOEE. This is consistent with negligible charge current generation by the spin/OAM pumping for FM/Cu/Al_2O_3 (FM=CoFe, Fe, Ni or $Ni_{80}Fe_{20}$(Py)) structures in our previous study[1]. And this result implies that the OAM escaping from the Cu/Al_2O_3 interface is much more effective than the relaxation at the interface likely due to a small energy barrier between the Cu/Al_2O_3 interface and the Cu bulk[2,5].

S3. OT for naturally oxygen-incorporated Py/Cu/Al_2O_3 and Py/Cu

One of the most noticeable OT's property is the strong FM dependence. Particularly, many of studies report small OT for adoption of Py as a FM material[1,6,7]. Firstly we prepare naturally oxygen-incorporated Py/Cu/AlO_X structures by the same preparation manner with the Series 6.7, 10.5 and 11.0. OT for the Py/Cu/AlO_X structures as a function of the exposure time is shown in Fig. S3(a). Consistent with literature, the OT is always close to zero independent of the annealing temperature. Next, we deposited a Py/Cu structure without a capping layer. Just after the deposition of the Py/Cu structure, we started the OT measurement. The zero exposure time corresponds to moment that the Py/Cu structure is pulled out from the evaporator. The maximum exposure time is 19.5 h, but we never obtain considerable torque in this system. Contrasting OT by the selection of FM stresses that the considerable torque in the CoFe/Cu/AlO_X structures dominantly comes from the role of the OAM.

S4. Material characterization - HAADF-STEM observation and EDS mapping

The HAADF-STEM observation and the EDS analysis were carried out for selected samples such as 10 min and 6 h oxygen-incorporated sample in Series 6.7, and 10 min, 2 h and 6 h oxygen-incorporated sample in Series 10.5. Similarly, same observation/analysis were carried out for selected samples such as as-deposited and 300 °C annealed samples.

HAADF-STEM observation and EDS analysis was done by using FEI Titan G2 80–200 at 200 kV, and samples for STEM-EDS analysis were prepared by using a focused ion beam (FIB) with a scanning electron microscopy (SEM) system, FEI Helios G4UX. All the EDS line concentration profiles are averaged value for 35 nm-width regions. An example for the EDS analysis with a complete compositional line profile is displayed in Fig. S4 (a).

STEM images for 10 min and 6 h oxygen-incorporated samples in Series 6.7 are displayed in Fig. S4(b). Also STEM images for as-deposited and 300 °C annealed samples are displayed in Fig. S4(c).

Complete EDS line concentration profiles are presented in Fig. S5.

S5. OT dependency vs gradient of the oxygen accumulation

We consider a universal OT curve as a function of the oxygen accumulation gradient nearby the CoFe/Cu interface (Fig. 3(d)). We select a 1.5 nm-length region from the peak of the oxygen's oxygen EDS concentration profile in rich-CoFe area. The slope of the oxygen EDS concentration profile in this region is defined 'gradient'. As mentioned in main text, it reveals a tendency that OT is large as the value of the gradient is small. Surely, this graph cannot be perfectly universe considering that the oxygen accumulation is not a sole factor to determine the magnitude of the OT.

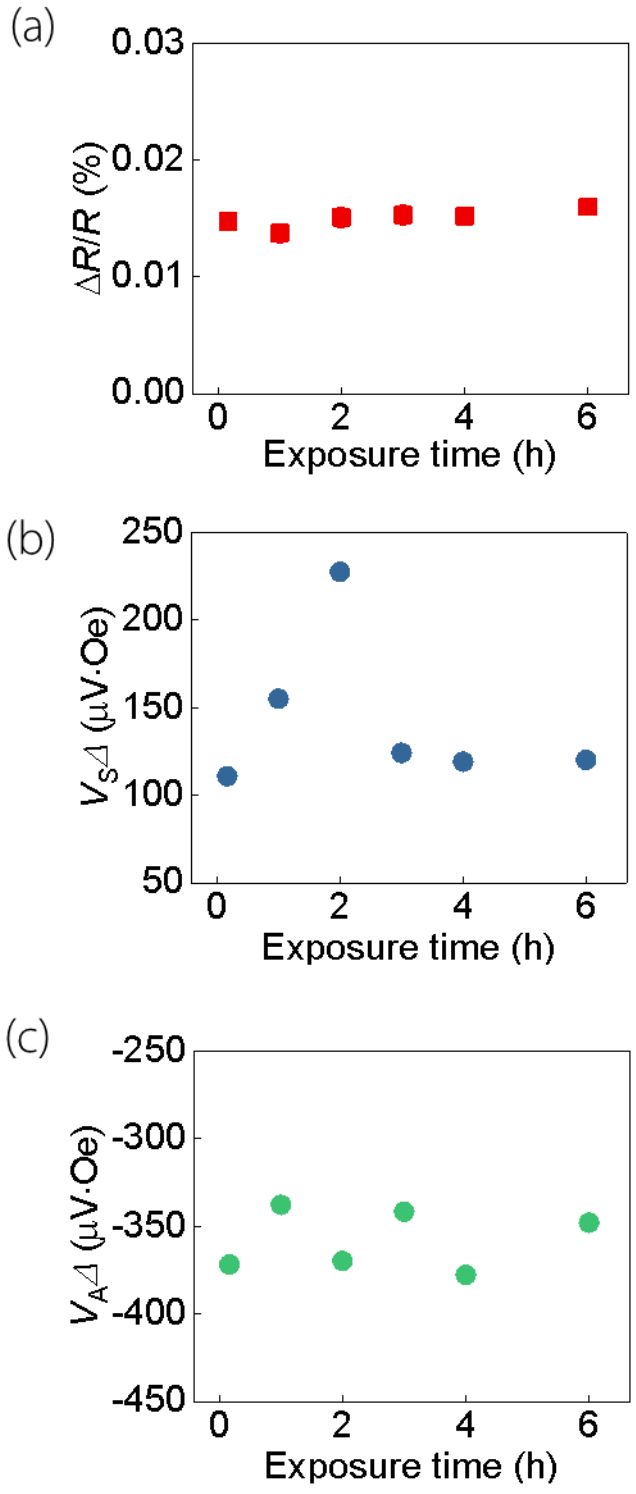

Fig. S1 (a) Total MR as a function of the exposure time. (b), (c) $V_S\Delta$ (b) and $V_A\Delta$ (c) as a function of the o exposure time.

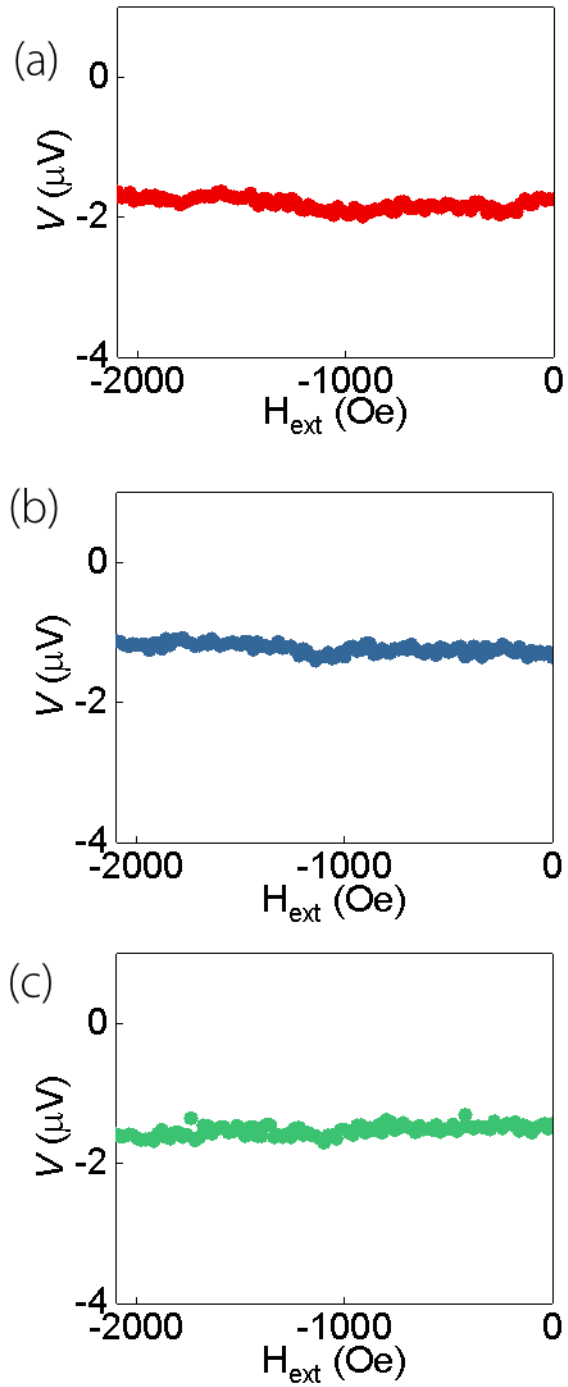

Fig. S2 (a), (b), (c) Measured voltage by the spin/OAM pumping for 10 min (a), 2 h (b), and 4 h (c) exposed structure among Series 10.5. Commonly the spin/OAM pumping is generated by 20 dBm-10 GHz excitation.

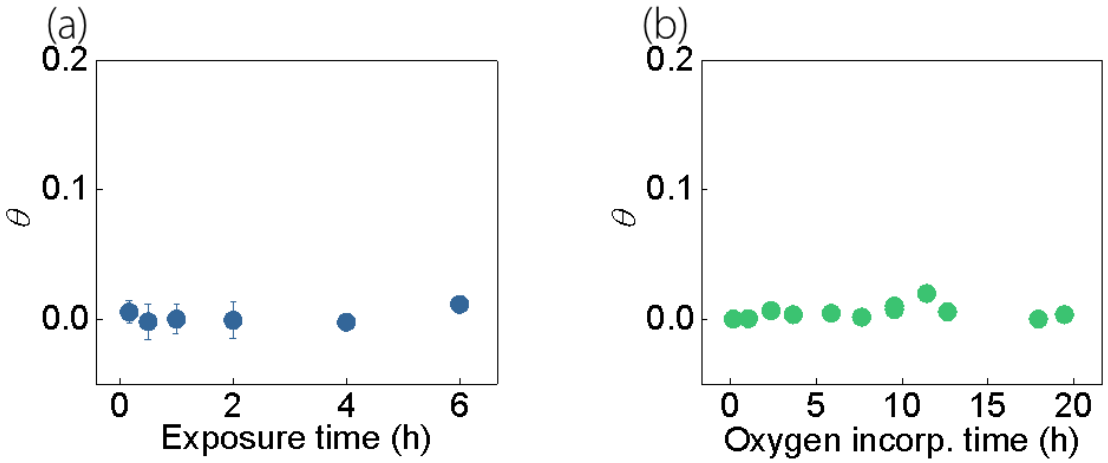

Fig. S3 (a) OT for Py/Cu/Al_2O_3 structures as a function of the exposure time. (b) OT for Py/Cu structure as a function of the exposure time.

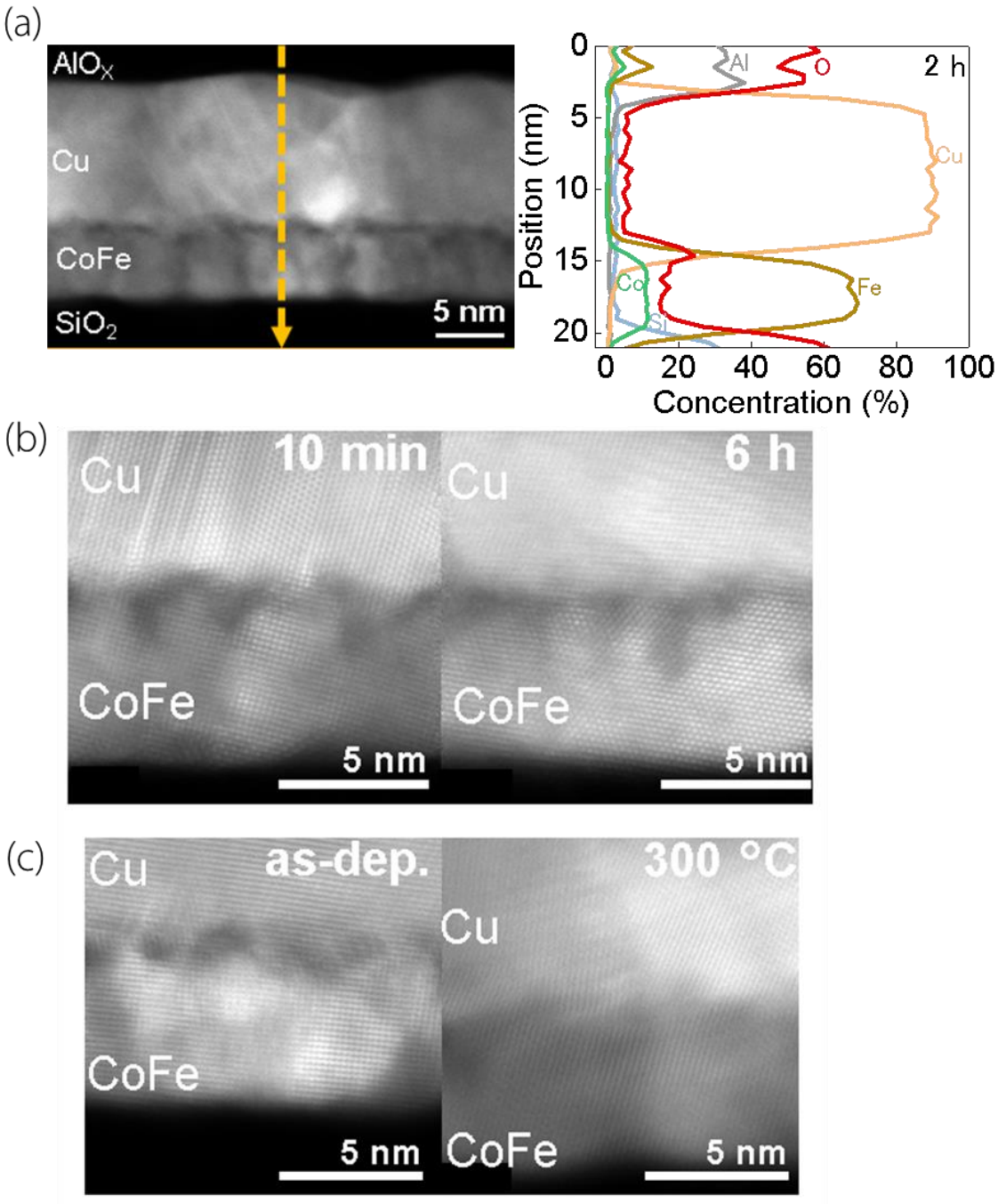

Fig. S4 (a) An example of EDS analysis. HAADF-STEM image (left) and EDS map with complete line concentration profile (right) for 2 h oxygen-incorporated sample in Series 10.5. (b) HAADF-STEM images for 10 min (left), and 6 h (right) oxygen-incorporated samples in Series 6.7. (c) HAADF-STEM images for as-deposited (left) and 300 °C annealed (right) samples.

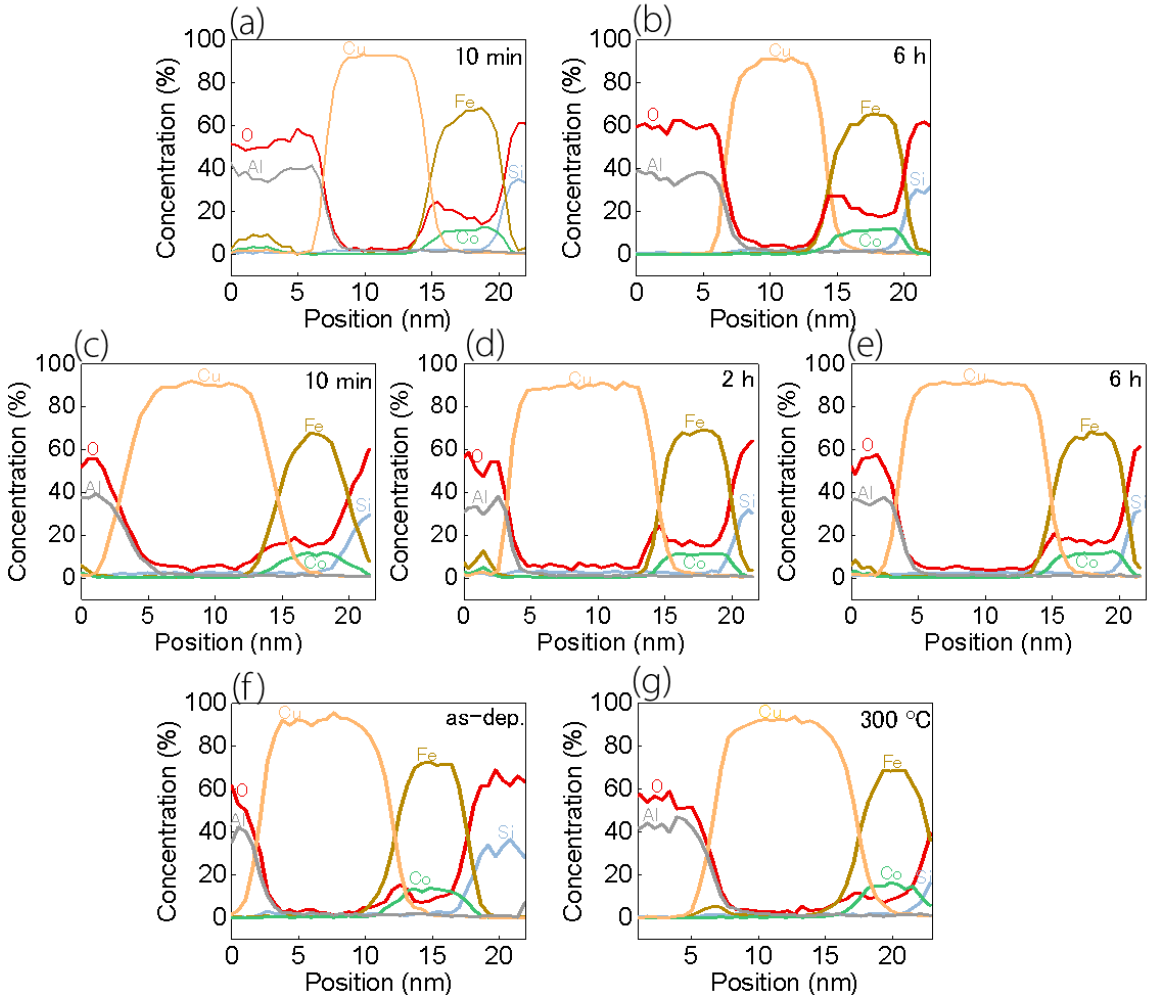

Fig. S5 Complete EDS line profile. Data for 10 min (a) and 6 h (b) exposed sample among Series 6.7 are shown. Data for 10 min (c), 2h (d) and 6 h (e) exposed sample among Series 10.5 are shown. Data for as-deposited (f) and 300 °C annealed (g) sample are shown.

1 Kim, J. *et al.* Nontrivial torque generation by orbital angular momentum injection in ferromagnetic-metal/Cu/Al_2O_3 trilayers. *Phys. Rev. B* **103**, L020407 (2021).

2 Kim, J. *et al.* Evaluation of bulk-interface contributions to Edelstein magnetoresistance at metal/oxide interfaces. *Phys. Rev. B* **96**, 140409 (2017).

3 Santos, E. *et al.* Inverse Orbital Torque via Spin-Orbital Entangled States. *arXiv:2204.01825* (2022).

4 Kondou, K. *et al.* Influence of inverse spin Hall effect in spin-torque ferromagnetic resonance measurements. *Appl. Phys. Express* **9**, 023002 (2016).

5 Zhang, S. & Fert, A. Conversion between spin and charge currents with topological insulators. *Phys. Rev. B* **94**, 184423 (2016).

6 Liao, L. *et al.* Efficient orbital torque in polycrystalline ferromagnetic-metal/Ru/Al_2O_3 stacks: Theory and experiment. *Phys. Rev. B* **105**, 104434 (2022).

7 Hayashi, H. *et al.* Observation of long-range orbital transport and giant orbital torque. *arXiv:2202.13896* (2022).